DOI: 10.5281/zenodo.3784343
CZU 681.586

MICROHEATERS FOR COPPER OXIDE-BASED GAS SENSORS

Nicolai Ababii[1,2], ORCID: 0000-0001-5046-8611,
Viorel Trofim[1], ORCID: 0000-0002-6620-3076,
Oleg Lupan[1,2*], ORCID: 0000-0002-7913-9712

[1] Department of Microelectronics and Biomedical Engineering, Technical University of Moldova, 168 Stefan cel Mare Av., MD-2004 Chisinau, Republic of Moldova
[2] Center for Nanotechnology and Nanosensors, Technical University of Moldova, 168 Stefan cel Mare Av., MD-2004 Chisinau, Republic of Moldova
*Corresponding author: Oleg Lupan, *oleg.lupan@mib.utm.md*

Received: 04. 10.2020
Accepted: 05.12.2020

Abstract. This paper describes two procedures developed for obtaining microheaters for copper oxide-based gas sensors. Different types of substrates (glass, SiO_2/Si and ceramic) are investigated, as well as different configurations of geometric parameters for meandering heating elements. It is shown that microheaters made on glass, ceramic and SiO_2/Si substrates can survive up to a temperature of ~ 400 °C, which allows their integration for applications in gas sensing devices to maintain necessary operating temperature.

Keywords: *microheater, copper oxide, gas sensors, glass substrate, semiconductors.*

Introduction

In recent years, gas sensors based on oxide semiconductors such as copper oxide [1], have an impressive progress, as their market demands are quite high due to necessity in detection of the toxic and flammable gases, as well as their low-cost, functionality and sensor performance. However, for their reliable operation, it is necessary to elevate the operating temperatures up to 200-350 °C, in order to facilitate physical-chemical reactions on the semiconducting oxide active surface [2, 3]. For these reasons, there is a need for a new micro-heaters design, which possesses a uniformity of thermal distribution, low energy consumption and low prices, as well as the compatibility with the sensor technology for seamless integration into a portable device or a microsystem [4]. Laconte *et al.* presented a configuration of the microheater that includes most of the properties listed above, the polysilicon based microheater demonstrated a temperature rise of 400 °C with a consumption of 20 mW [4]. Suehle *et al.* have developed polysilicon based micro-heaters, obtaining a temperature of 400 °C at 47 mW [5]. Baroncini *et al.* obtained a temperature of ~ 400 °C with the consumption of 65 mW, based on a micro-heater with double coil of Pt [6]. Briand *et al.* have developed a Pt-based microheater on silicon oxide substrate, and obtaining 300 °C at 75 mW [7]. Mo *et al.* have developed a Pt/Ti micro-heater on silicon

oxide substrate, obtaining 400 °C at 9 mW [8]. Udrea *et al*. obtained a temperature of 350 °C at 100 mW consumption by using new types of microheaters [9].

This paper reports on nichrome–based microheaters on glass, ceramic and silicon oxide substrate for copper oxide-based gas sensors, which can maintain a temperature of 350 °C without damaging the substrate. We also would like this microheater to be cost-efficient and can be produced by a simple fabrication technology.

Experimental

Thin films for microheaters fabrications were made using two technological processes, namely: (1) deposition of metals in vacuum (by using installation VUP-4), and (2) by evaporation of metals and their mixtures in vacuum and photolithography.

The first approach for the fabrication of the microheaters elements is based on deposition of the nichrome thin films in vacuum on a glass, ceramic and SiO_2/Si substrates. The deposition was performed in vacuum ($1.3 \cdot 10^{-2}$ Pa). The process starts from cleaning the substrate in HNO_3 or H_2SO_4, then it is rinsed with deionized water and finally cleaned with ethanol. On the cleaned substrate, the mask with the meander heating elements is overlaid (Figure 1, step 1) and the mask+substrate is introduced into the VUP -4 installation, pumped down to high vacuum ($1.3 \cdot 10^{-2}$ Pa). The substrate holder is then heated to 200 °C to improve the adhesion of the substrate. Then 120-150 mg Ni-Cr alloy (nichrome wire) was placed on the tungsten evaporator and vaporized (Figure 1, step 2). Afterwards, the overlay of the contact mask of the microheater, on the substrate already having the Ni-Cr alloy heater elements, being reintroduced into the VUP-4 installation (Figure 1, step 3), creating a high vacuum, the substrate is heated up to 200 °C and the nichrome (120-150 mg) is deposited for contacts (Figure 1, step 4) and next is deposited copper or nickel contact material with a mass of 180-200 mg (Figure 1, step 5).

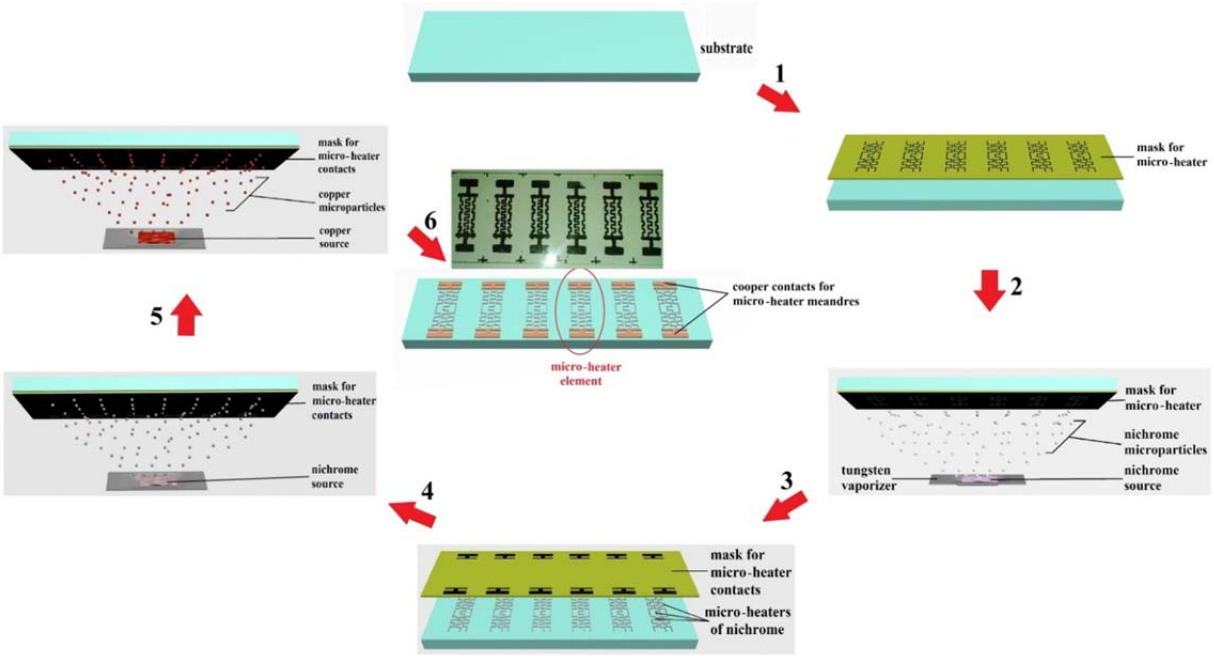

Figure 1. Overall technological process for the development of the micro-heating elements: (1) substrate is covered with a meander shadow mask; (2) Ni-Cr alloy (nichrome powder) was placed on the tungsten evaporator and vaporized; (3) substrate is covered with a shadow mask for creating microheater contacts; (4) vaporized Ni-Cr alloy contacts or (5) vaporized Cu contacts; (6) final structure-microheater elements.

Finally (Figure 1, step 6), substrate with several heating elements is removed from VUP-4 after temperature was lowered to 20 °C.

The second approach for fabrication of such microheaters is based on photolithography, which starts from the deposition of a layer of nichrome on a glass, ceramic or SiO_2 (300 nm)/Si substrate, which is made by vacuum deposition using the VUP-4 vacuum system. The nichrome layer is deposited as follows: a high vacuum is formed, after which the substrate is heated to a temperature of 200 °C, the nichrome is vaporized on the surface of the substrate, resulting in a layer of nichrome with a resistance of several Ohms. The process of photolithography begins with the deposition of the AZ 701 MIR type photoresist on the substrate with the already deposited nichrome film by spin-coating at a speed of 1000 rpm. After applying the photoresist, the sample is dried on the infrared drying line at 90 °C for 3 min. After the photoresist has dried, the sample is exposed to the ultraviolet illumination for 60 s. After exposure, the photoresist is placed into the KOH solution, and then the heating elements are projected onto the nickel layer on the substrate. The following step is to dry the sample at 110 °C for 3 minutes. After drying, the nickel layer is etched, thus obtaining the configuration of the heating elements on the substrate with a resistance of 30-80 Ohm, depending on the thickness of the nichrome layer.

For the fabrication of microheaters, the different configurations of nichrome film heating elements were used. The necessary masks were fabricated based on copper foils with geometrical parameters shown in Figure 2. All microheaters are composed of meanders with different thickness and configuration, connected in parallel with width of 0.3 mm.

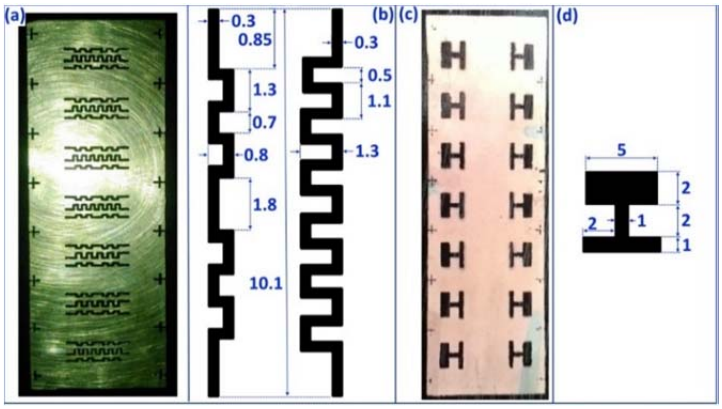

Figure 2. (a) Optical image of the mask used for micro-heaters fabrication, which is made from a thin copper foil. (b) Geometrical parameters of the heating elements (units are in mm) for mask from (a). (c) Mask for contacts deposition for heaters shown in (a); and (d) geometrical parameters of one contact.

Following the second technological approach based on photolithography, the thinner meanders of 100 and 200 μm were obtained, as well as of 500 μm and 1 mm with geometrical parameters shown in Figure 3. In this case, when the meander width is 100 μm, 200 μm, 500 μm and 1mm, we connect 18, 8, 5 and 3 meanders in parallel respectively, to form our microheaters.

The thermal properties of the microheater was measured using a home-made installation, based on microprocessor controlled electrical source and temperature sensor shown in Figure 4.

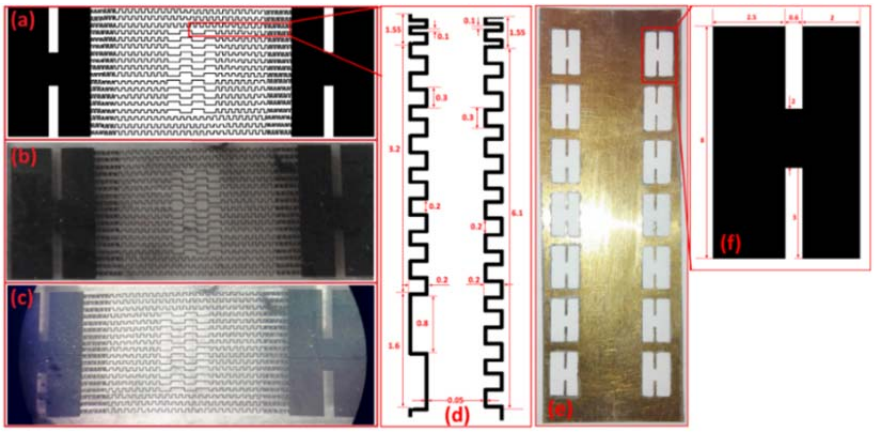

Figure 3. The deposited micro-heaters using mask #3: (a) The design of microheater and meanders; (b) Optical image of a real micro-heater element deposited onto glass substrate taken using the digital camera; (c) Optical image of the same micro-heater taken through the optical microscope; (d) The geometrical parameters of the heating elements (the units are presented in mm); (e) The optical image of the mask used for deposition of contacts for heating elements elaborated from the thin copper foil; (f) Geometrical parameters of the used contact for heating element.

The measurement process is as follows: the required voltage is manually applied from the source (step 1). Using the voltmeter, we measure the voltage applied to the micro-heater and the voltage that is from the source for the measurements, to be as precise as possible (step 2 and 3). With temperature sensor "PT100" the temperature of the substrate surface with the deposited micro-heater were measured and manually recorded the data (step 4). In order to avoid external influence on the measurements, the micro-heaters are measured in a closed chamber (step 5). To investigate in more details morphology of the deposited layers were used SEM REMZEISS (3.0 kV, 5.0 μA).

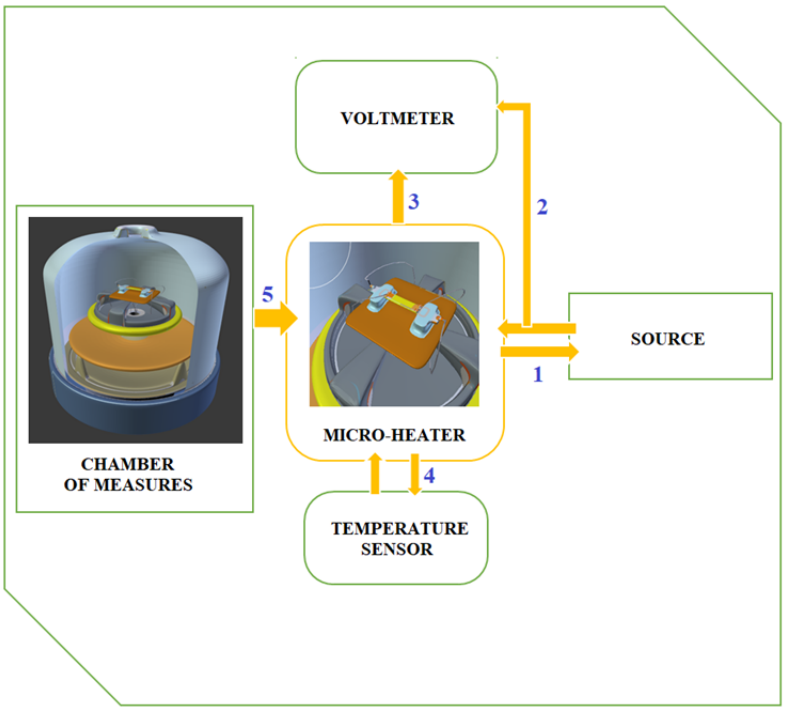

Figure 4. Microheater measuring system.

Results and Discussion

In this section, the morphology of deposited layers, the best type of substrate, optimal geometrical parameters, power consumption and the optimal temperatures reached will be discussed.

For the first approach the morphology is discussed below. Figure 5(a) shows the optical image of two microheater elements fabricated on the glass substrate. According to SEM studies, at these magnifications, no cracks or visible defects have been observed, and all layers are deposited very well on the glass substrate. To investigate the deposited layer in more details with width of the element of ≈ 600 μm, the SEM image of the single heating element is presented in Figure 5(b).

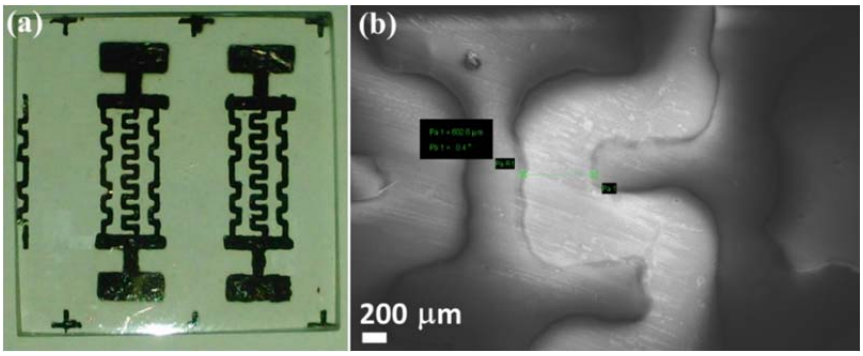

Figure 5. (a) Optical digital image of a real micro-heater; and (b) SEM image of microheater on glass substrate.

As it can be seen, no defects such islands, scars or cracks can be observed. It can be explained by probably shadowing type of deposition. However, meanders are not interconnected between each over.

Figure 6(a) shows the optical and Figure 6(b) presents SEM images of the microheater deposited on ceramic substrate, heated at temperature of 200 °C, with micro-heaters meander of nichrome (60 mg) and nickel contacts. It can be observed that nichrome film is relatively uniform and homogeneous. Meanders has width around 418-491 μm throughout its length, on the surface film does not linger defects such islands, scars or cracks that would prevents the current passing through it.

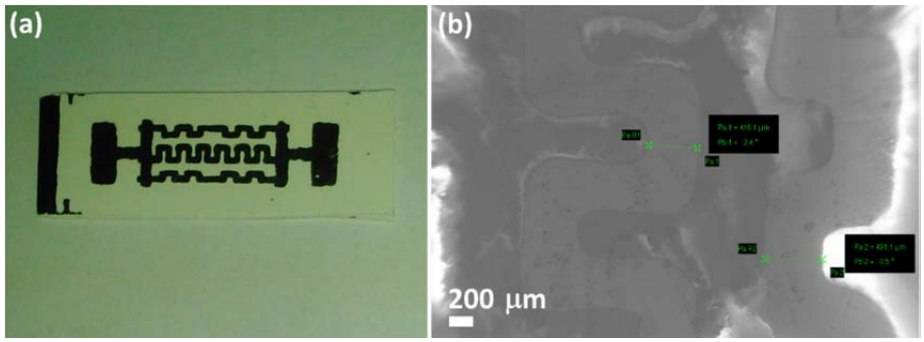

Figure 6. (a) Optical digital image; and (b) SEM image of microheaters on ceramic substrate with nickel contacts.

In Figure 7 the optical (a) and SEM (b) images of the micro-heaters deposited in vacuum on SiO_2 (300 nm)/Si substrate are presented. Meanders has width around 450-580 μm throughout its length, on the film surface no defects such islands, scars or cracks were observed.

The results based on the second approach to fabricate such microheaters elements are shown below.

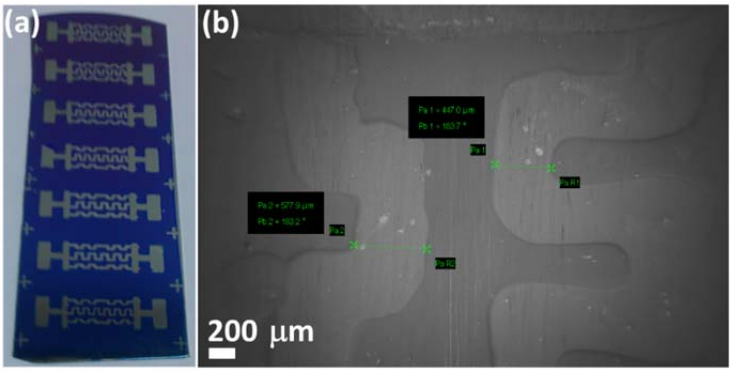

Figure 7. (a) Optical digital image; and (b) SEM image; of microheaters on ceramic substrate with nickel contacts.

Figure 8(a) shows the optical image of six microheaters fabricated on the glass substrate with the width of the meander of 100 μm on a glass slide. As it can be seen, at these dimensions, no cracks or visible defects can be observed even at more detailed investigations under optical microscope, and all layers are deposited very well on glass substrates. To investigate in more details the deposited layers; we also take the SEM images of the single heating element, which is presented in Figure 8(b). As can be seen, no defects such as islands, scars or cracks that would prevents the current passing through it, can be observed. According to the SEM images, the thickness of the meanders is ~ 80 – 90 μm, see Figure 8(b).

Figure 9 (a) shows the optical image of six microheater elements fabricated on the glass substrate with the width of 200 μm. As it can be seen, at these dimensions, no cracks or visible defects can be observed, and all layers are deposited very well on glass substrate. To investigate in more details the deposited layer, the SEM image of the single heating element is presented in Figure 9(b) showing nichrome meander and nickel contact region (left).

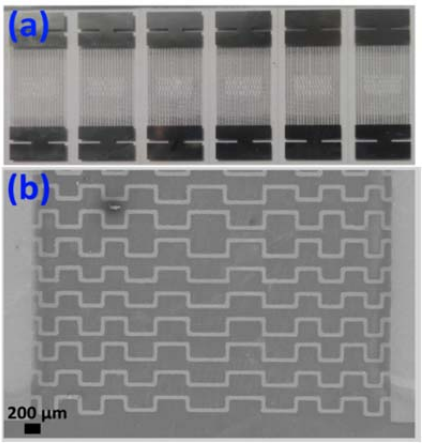

Figure 8. (a) Optical digital image of a real microheater developed; and (b) SEM image of microheater on glass substrate with the width of about 100 μm.

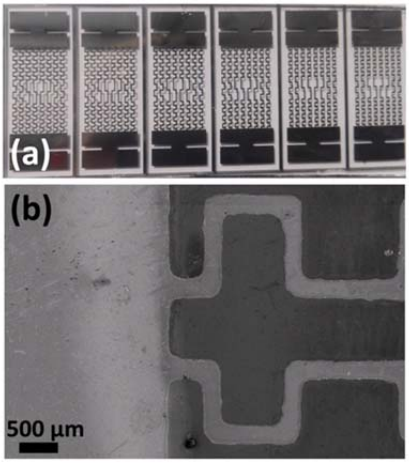

Figure 9. (a) Optical digital image of six real microheaters on glass substrate; and (b) SEM image of a microheater on glass substrate with the width of 200 μm.

The thermal characteristics of micromachined gas sensors have to be optimized with respect to low power consumption, well-controlled temperature distribution over the sensing layer and fast transient response, if the sensor is intended to be temperature modulated [10]. Generally, the heat transfer occurs due to heat conduction, heat convection and radiation [10]. Above and below the substrate heat transfer occurs through heat

conduction and heat convection through the surrounding atmosphere [10]. Additionally, radiation has to be considered [10, 11]. Due to a high number of influencing factors, the calculation of heat transfer, heat loss and temperature distribution is not easy. However, a simple model can be presented in order to investigate the most important parameters which can influence the heating elements. Simon *et al*. assumed that if the different components of heat flow is additive, then the total heat flow (Q_{tot}) in vacuum (where only one has to deal with heat losses due to conduction along the substrate and radiation) can be expressed as follows [10]:

$$Q_{tot} = G_{sub}\lambda_{sub}\left(T_{hot} - T_{amb}\right) + G_{air}\lambda_{air}\left(T_{hot} - T_{amb}\right) + G_{rad}\sigma\varepsilon\left(T_{hot}^4 - T_{amb}^4\right) + \Delta x \quad (1)$$

where the first term of equation describes the heat conduction through the substrate, the second indicates on the heat conduction through the ambient air, the third is heat losses due to radiation and the last term accounts for unknown heat losses including free convection [10, 11]. G_{sub}, G_{air} and G_{rad} are constants depending on geometrical factors of the substrate. T_{hot} and T_{amb} represent the temperatures of the substrate under the heater element and of the ambient, respectively. λ_{sub} and λ_{air} are the thermal conductivities of the substrate and surrounding ambient air, respectively. ε and σ is the emissivity and the Stefan-Boltzmann constants, respectively. If we assume that substrate thickness is several μm, which is not the case of glass substrate, we can assume that heat conduction for the substrate (Q_{sub}) can be expressed as follows [10]:

$$Q_{sub} = \frac{\left(\lambda_{sub} A\right)\left(T_{hot} - T_{amb}\right)}{L} \quad (2)$$

$$G_{sub} = \frac{A}{L} \quad (3)$$

where L is the length of substrate and A is the area of substrate. In the case of glass substrate, where the thickness is ~ 1 mm, the three-dimensional model needs to be elaborated, which is more complex. If to suspend a substrate with 4 special beams, forming a membrane, the heat conduction for the substrate would be expressed as [10]:

$$Q_{sub} = \frac{4\left(\lambda_{sub} A_{beam}\right)\left(T_{hot} - T_{amb}\right)}{L} \quad (4)$$

$$G_{sub} = \frac{4A_{beam}}{L} \quad (5)$$

where A_{beam} is the area of the beam which suspends the membrane on which the heater is placed.

Also, a simpler model of membrane was presented by Sberveglieri *et al*. [12], where in order to reduce the model to one-dimensional, a conventional square membrane was replaced by a round one [10]. This leads to a one-dimensional heat conduction problem in cylindrical coordinates which can be easily solved as follows [8]:

$$Q_{sub} = \frac{2\pi\lambda_{sub}\left(T_{hot} - T_{amb}\right)}{\ln\left(r_a / r_i\right)} \quad (6)$$

$$G_{sub} = \frac{2\pi d}{\ln(r_a / r_i)} \tag{7}$$

where r_a and r_i is the radii of the heated area of membrane, and general radii of membrane, respectively, while d is the thickness of membrane. Length to width ratio of the suspension beams, respectively, the relation r_a=r_i should additionally be chosen as large as possible to minimize heat losses [10, 12].

By placing the heater element deposited on substrate in air, the heat loss will occur mainly by two different mechanisms, namely convection and conduction [10]. Convection can either be caused by external forces or it can be the result of temperature differences which lead to density variations in the gravitational field and thus to buoyancy forces [10]. The former case leads to heat transfer called forced convection, the latter is called free or natural convection [10]. When there is no convection, heat is transferred only by conduction [10]. In this case the heat loss can be estimated as follow [10, 11]:

$$Q_{cond} = \frac{4\pi\lambda_{air}(T_{hot} - T_{amb})}{1/r_i - 1/r_a} \approx 4\pi r_i \lambda_{air}(T_{hot} - T_{amb}) \tag{8}$$

$$G_{air} \approx 4\pi r_i \tag{9}$$

Thus, to optimize the power consumption the heated area represented by the inner radius r_i should be minimized as much as possible. The heat loss due to radiation can be expressed as follow, with assumption that the heated membrane area behaves like a gray emitter, i.e. the degree of emission of the heated membrane is set equal to the degree of absorption [10]:

$$Q_{rad} = G_{rad}\sigma\varepsilon(T_{hot}^4 - T_{amb}^4) \tag{10}$$

Heat losses due to radiation increases with heated membrane area. Generally, the heat losses due to radiation amount only a few percent of the total heat loss [10, 12 - 14] but due to the T^4-dependency they should be considered with care if very high sensor operation temperatures are applied.

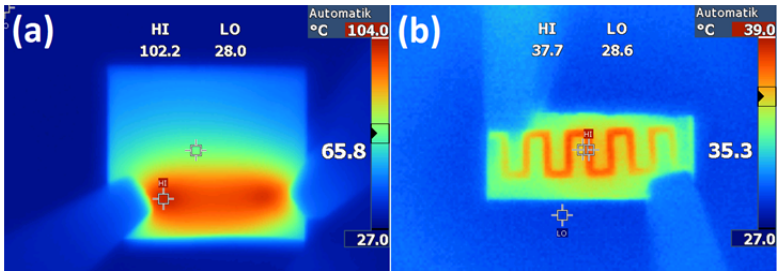

Figure 10. The temperature distribution of bottom glass substrate: (a) without nanostructures deposited film; and (b) with the CuO nanostructures deposited film and with gold contacts on top.

The heat distribution of the microheater at the glass substrates shows in Figure 10, where a uniform distribution across the substrate is observed. From the bottom image of the glass substrate with the CuO nanostructures deposited film and with gold contacts an excellent temperature distribution demonstrates the efficacy of the microheater.

There were deposited micro-heater elements with the width of 200 μm, after which the CuO nanostructures were deposited and thermally treated at 425 °C, thus, a microheater

temperature of 400 °C with the voltage applied of 27 V and a power of 9,5 W was obtained (see Figure 11).

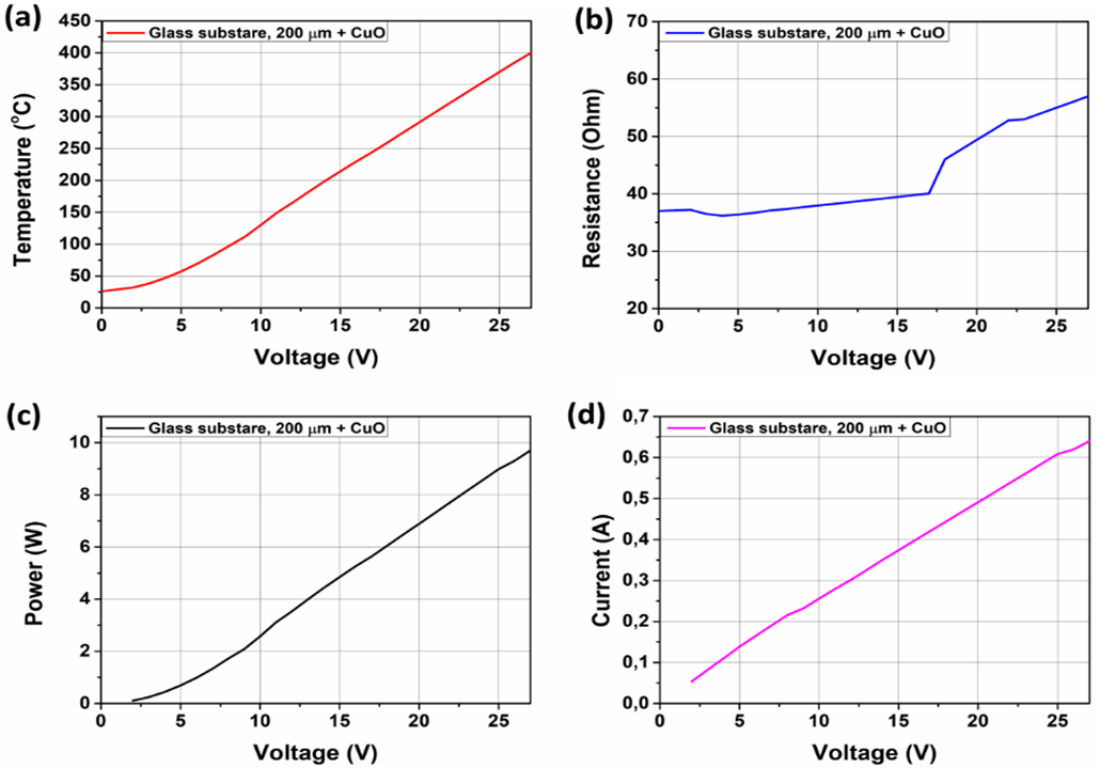

Figure 11. The characterization of micro-heater elements with thickness of meander of 200 μm deposited on glass substrate and with deposition of CuO nanostructured film: (a) Temperature dependence of voltage front; (b) Resistance dependence of voltage front; (c) Power dependence of voltage ramp; and (d) Current dependence of voltage front to sample deposited on glass with nickel contacts and the CuO nanostructures deposited film and afterwards it was heat treated at 425 °C.

Thus, nichrome microheaters deposited on glass substrate (with CuO nanostructures film) and gold contacts (Figure 12(a), curve 2 and Figure 12(b), curve 3 and 4), are more suitable for real applications in gas sensing devices.

Further investigations on thickness and geometrical parameters of microheaters are needed for optimization of power consumption and lowering of needed DC bias.

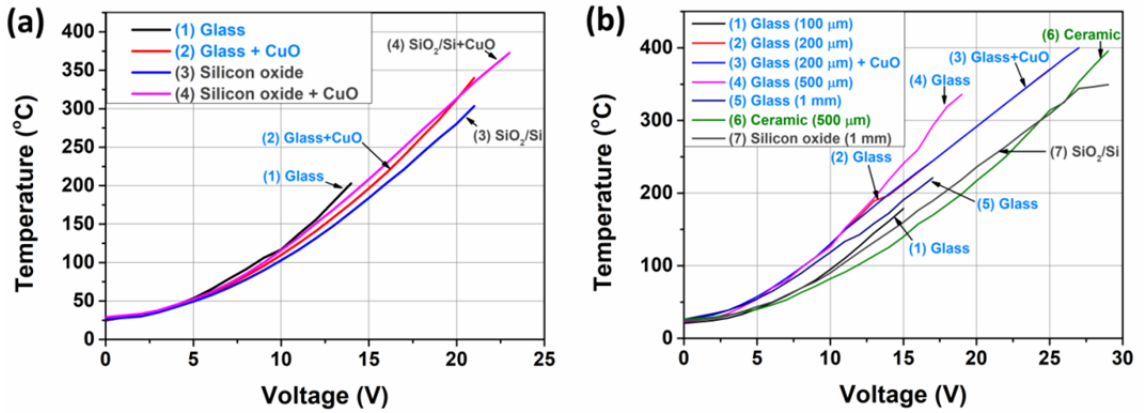

Figure 12. (a) Comparative graph of temperature dependence versus voltage of micro-heaters by vacuum deposition process on glass and silicon oxide substrates without nanostructures deposited film and with the CuO nanostructures deposited film and with gold contacts; (b) Comparative graph of temperature dependence versus voltage of micro-

heaters by photolithography process on glass (100 μm; 200 μm; 200 μm + CuO; 500 μm and 1 mm), ceramic (500 μm) and silicon oxide substrates (1 mm).

Conclusions

According to the obtained results we can mention that microheaters made on silicon oxide and ceramic substrate are the most successful due to the ability of generating the operating temperature up to 400 °C, but this requires a voltage up to 29 V resulting in a power consumption of about 10 W, respectively, which is not optimal for practical applications. However, gas sensors based on copper oxide from literature demonstrate the best gas sensing results are with the optimal operating temperature in range of 200 °C – 350 °C. It fits perfectly to parameters of our elaborated microheaters on glass substrate with the width of the meanders of 200 μm (200 °C – 350 °C), especially for experimental samples, which already were measured with CuO nanostructures film on top of microheater that showed a heating temperature of 400 °C.

Acknowledgments

This research was sponsored in part by the NATO Science for Peace and Security Programme (SPS) under grant G5634 „Advanced Electro-Optical Chemical Sensors" AMOXES.

References

1. Siebert L., Lupan O., Mirabelli M., Ababii N., Terasa M.-I., Kaps S., Cretu V., Vahl A., Faupel F., Adelung R. 3D-Printed Chemiresistive Sensor Array on Nanowire CuO/Cu_2O/Cu Heterojunction Nets. In: *ACS Appl. Mater. Interfaces*. 2019, 11, pp. 25508–25515.
2. Lupan O., Postica V., Hoppe M., Wolff N., Polonskyi O., Pauporté Th., Viana B., Majérus O., Kienle L., Faupel F., and Adelung R. PdO/PdO_2 functionalized ZnO:Pd films for lower operating temperature H_2 gas sensing. In: *Nanoscale*, 2018, 10, pp. 14107-14127.
3. Lupan O., Postica V., Wolff N., Su J., Labat F., Ciofini I., Cavers H., Adelung R., Polonskyi O., Faupel F., Kienle L., Viana B., Pauporté Th. Low-Temperature Solution Synthesis of Au-Modified ZnO Nanowires for Highly Efficient Hydrogen Nanosensors. In: *ACS Appl. Mater. Interfaces,* 2019, 11 (35), pp. 32115-32126.
4. Laconte J., Dupont C., Flandre D.s and Raskin J.-P. SOI CMOS Compatible Low-Power Microheater Optimization for the Fabrication of Smart Gas Sensors. In: *IEEE SENSORS JOURNAL*, 2004, 4 (5), pp. 670-680.
5. Suehle J. S., Cavicchi R. E., Gaitan M. and Semancik S. Tin Oxide Gas Sensor Fabricated Using CMOS Micro-Hotplates and In –Situ Processing. In: *IEEE Electron Device Letters*, 1993, 14 (3), pp. 118-120.
6. Baroncini M., Placidi P., Cardinali G.C., Scorzoni A. Thermal characterization of a microheater for micromachined gas sensors. In: *Sensors and Actuators A,* 2004, 115, pp. 8–14.
7. Briand D., Krauss A., Schoot B., Weimar U., Barsan N., Gopel W., Rooij N.F. Design and fabrication of high-temperature micro-hotplates for drop-coated gas sensors. In: *Sensors and Actuators B,* 2000, 68, pp. 223–233.
8. Mo Y., Okawa Y., Tajima M., Nakai T., Yoshiike N., Natukawa K. Micro-machined gas sensor array based on metal film micro-heater. In: *Sensors and Actuators B*, 2001, 79, pp. 175-181.
9. Udrea F., Gardner J. W., Setiadi D., Covington J. A., Dogaru T., Lu C. C., Milne W. I. Design and simulations of SOI CMOS micro-hotplate gas sensors. In: *Sensors and Actuators B,* 2001, 78, pp. 180-180.
10. Simon I., Barsan N., Bauer M., Weimar U. Micromachined metal oxide gas sensors: opportunities to improve sensor performance. In: *Sensors and Actuators B,* 2001, 73, pp. 1-26.
11. Hwang W.-J., Shin K.-S., Roh J.-H., Lee D.-S., Choa S.-H. Development of Micro-Heaters with Optimized Temperature Compensation Design for Gas Sensors. In: *Sensors*, 2011, 11, pp. 2580-2591.
12. Sberveglieri G., Hellmich W., Muller G. Silicon hotplates for metal oxide gas sensor elements. In: *Microsyst. Technol.*, 1997, 3, pp. 183-190.
13. Goetz A., Gracia I., Cane C., Lora-Taniayo E., Horrillo M., Getino G., Gracia C., Gutierez J. A micromachined solid state integrated gas sensor for the detection of aromatic hydrocarbons. In: *Sens. Actuators B*, 1997, 44, pp. 483-487.
14. Lee D., Chung W., Choi M., Back J. Low-power micro gas sensor. In: *Sens. Actuators B,* 1996, 33, pp. 147-150.